agronomy

Article

Abnormal Calcium Accumulation and ROS Homeostasis-Induced Tapetal Programmed Cell Death Lead to Pollen Abortion of Petaloid-Type Cytoplasmic Male Sterility in *Camellia oleifera*

Xiaolei Gao [1,2], Ying Yang [1,2], Jiawei Ye [1,2], Huan Xiong [1,2], Deyi Yuan [1,2] and Feng Zou [1,2,*]

[1] Key Laboratory of Cultivation and Protection for Non-Wood Forest Trees, Ministry of Education, Central South University of Forestry and Technology, Changsha 410004, China; 20211100076@csuft.edu.cn (X.G.); 20221100075@csuft.edu.cn (Y.Y.); 20211100079@csuft.edu.cn (J.Y.); t20202024@csuft.edu.cn (H.X.); t20061123@csuft.edu.cn (D.Y.)

[2] Hunan Key Laboratory of Colleges and Universities of Oil Tea Breeding, Central South University of Forestry and Technology, Changsha 410004, China

* Correspondence: t20142217@csuft.edu.cn

Abstract: Cytoplasmic male sterility (CMS) plays a crucial role in the utilization of heterosis. The petaloid anther abortion in oil tea (*Camellia oleifera* Abel.) constitutes a CMS phenomenon, which is of great value for the hybrid breeding of oil tea. However, as the mechanism of its CMS is still poorly understood, it is necessary to study the cytology and physiological characteristics of anther abortion. In this study, a *C. oleifera* cultivar, Huashuo (HS), and its petalized CMS mutant (HSP) were used as materials to explore this mechanism. Compared with HS, cytological analysis demonstrated that HSP showed early-onset tapetum programmed cell death (PCD) and an organelle disorder phenotype during the tetrad stage. In HSP, anthers exhibited elevated levels of calcium deposition in anther wall tissues, tapetum layers, and microspores, and yet calcium accumulation was abnormal at the later stage. The contents of hydrogen peroxide and MDA in HSP anthers were higher, and the activities of superoxide dismutase (SOD), peroxidase (POD), and catalase (CAT) were lower than those of HS, which resulted in an excessive accumulation of reactive oxygen species (ROS). Real-time quantitative PCR confirmed that the transcription levels of *CoPOD* and *CoCAT* genes encoding key antioxidant enzymes in HSP were downregulated compared with HS in early pollen development; the gene *CoCPK*, which encodes a calcium-dependent protein kinase associated with antioxidase, was upregulated during the critical period. Thus, we suggest that excessive ROS as a signal breaks the balance of the antioxidant system, and along with an abnormal distribution of calcium ions, leads to the early initiation of PCD in the tapetum, and ultimately leads to pollen abortion for HSP. These results lay a cytological and physiological foundation for further studies on the CMS mechanism, and provide information for breeding male-sterile lines of *C. oleifera*.

Keywords: cytoplasmic male sterility; petaloid anther; calcium homeostasis; ROS metabolism; tapetal PCD; gene expression; *Camellia oleifera*

check for updates

Citation: Gao, X.; Yang, Y.; Ye, J.; Xiong, H.; Yuan, D.; Zou, F. Abnormal Calcium Accumulation and ROS Homeostasis-Induced Tapetal Programmed Cell Death Lead to Pollen Abortion of Petaloid-Type Cytoplasmic Male Sterility in *Camellia oleifera*. *Agronomy* **2024**, *14*, 585. https://doi.org/10.3390/agronomy14030585

Academic Editor: Aisheng Xiong

Received: 3 February 2024
Revised: 9 March 2024
Accepted: 11 March 2024
Published: 14 March 2024

Copyright: © 2024 by the authors. Licensee MDPI, Basel, Switzerland. This article is an open access article distributed under the terms and conditions of the Creative Commons Attribution (CC BY) license (https://creativecommons.org/licenses/by/4.0/).

1. Introduction

Camellia oleifera, commonly known as the tea-oil tree, is a significant oil crop that is widely cultivated in China, South Korea, India, and Vietnam [1,2]. As one of the four major woody oil species in the world, *C. oleifera* seed oil possesses significant medicinal and nutritional value, and is rich in unsaturated fatty acids and bioactive compounds [3,4]. At present, the cultivation of elite cultivars with heterosis by hybrid breeding is an important way to increase the yield of *C. oleifera*. Hybrid breeding with male-sterile materials has been widely used in the agriculture field [5]. Using male-sterile material as a female parent can bypass the work of artificial sterilization in hybridization and greatly shorten the breeding

process. Male sterility can be classified as genic male sterility (GMS) or cytoplasmic male sterility (CMS) in higher plants, depending on inheritance or origin [6]. In CMS, layers of interaction between mitochondrial and nuclear genes control male specificity, occurrence, and the restoration of fertility [7]. Furthermore, CMS in crop species can be subdivided based on the phenotypic characteristics of the stamens, including the brown anther type and the petaloid stamen type [8]. In petaloid-type male sterility, the anther filament structure is replaced by petals or sepals [9]. Petaloid stability is found in many crop species, including *Brassica juncea* [9] and *Daucus carota* [8]. The petaloid-type CMS in *C. oleifera* 'X1' has also been reported in previous studies [10]. The anthers of petaloid-type male-sterile *C. oleifera* plants produce little or no pollen, which is helpful for leveraging heterosis as female parents [10,11]. Thus, understanding the mechanism of male sterility through the study of abortive anthers contributes to improving the traditional breeding strategies of *C. oleifera*.

Petaloid CMS has been extensively studied in many plant species. For instance, petaloid CMS in carrot was characterized by male organ abnormality caused by the homeotic conversion of stamens into greenish petals [12]. In the hau CMS line of *B. juncea*, stamens transform into thickened petal-like structures [13], and cytological analysis revealed that abnormal anther development in the hau CMS line was arrested during the differentiation of stamen archesporial cells [14]. An abnormal subcellular structure of pollen mother cells and delayed tapetum degradation were found in the CMS line SaNa-1A of *B. napus* [15]. As the innermost layer of the anther wall, the tapetum secretes enzymes that promote the release of microspores from the tetrad before it degenerates. The tapetum provides nutrients and various metabolites for pollen development, including sporopollenin, tryptophan precursors, sugars, and lipids [16]. The programmed cell death (PCD) of the tapetum is crucial for pollen maturation, and its remnants participate in pollen development processes. Early or delayed degradation of the tapetum layer can affect microspore development and lead to the male sterility of plants [17].

Many studies have suggested that the homeostasis of ROS is necessary for normal PCD of the tapetum, and that the autophagy of tapetal cells can be triggered by the abnormal homeostasis of ROS [17]. ROS are mainly produced by mitochondria, chloroplasts, and plasma membrane-associated NADPH oxidase, which is broken down into water and oxygen by an antioxidant system consisting of antioxidant enzymes, including superoxide dismutase (SOD), peroxidase (POD), and catalase (CAT) [18]. Thus, maintaining a dynamic balance between ROS production and breakdown in the anther is crucial, and any imbalance may lead to pollen abortion. In the 722HA CMS line of Kenaf, the abnormal development and early degradation of tapetum cells is accompanied by excessive ROS accumulation which impedes the normal development of microspores [19]. A similar phenomenon also appeared in the development of microspores in male-sterile line YS3038-A of TCMS wheat [20]. On the contrary, excessive ROS accumulation in CMS anthers of *B. napus* resulted in a delayed degradation of the tapetum, with a decrease in antioxidant enzyme activity and an increase in malondialdehyde (MDA) content [15].

Studies have shown that abnormal calcium (Ca^{2+}) distribution is related to anther abortion. During anther development in rice, a large amount of calcium deposits are accumulated in the tapetum and anther chamber, and in photoperiod-sensitive genetically male-sterile rice lines, the sterile anthers showed abnormal calcium distribution compared with fertile anthers [21]. Meanwhile, Ca^{2+} acts as a second messenger present in vacuoles, plastids, mitochondria, and the endoplasmic reticulum [22]. To avoid cytotoxicity caused by increased Ca^{2+} levels, plants encode different calcium-binding proteins that chelate and buffer cytoplasmic Ca^{2+}. EF-hand-containing proteins can actively bind and chelate cytoplasmic calcium, which plays a crucial role in mediating plant calcium signaling. These proteins include calcium-dependent protein kinases (CDPK/CPKs) and CPK-associated protein kinases (CRKs), and calcium- and calmodulin-dependent protein kinases (CCaMKs) and calmodulins (CaMs) [23]. Ca^{2+}-dependent protein kinase 5 (TaCPK5), located on the plasma membrane in wheat, can promote ROS production by inhibiting the activity of TACPK5-mediated catalase protein TaCAT1 [24].

Previous studies have reported that the petalized male sterility of *C. oleifera* may be related to premature or late degradation of the tapetum [10,11]. However, the physiology of calcium accumulation and reactive oxygen species during abortive anther development remains unclear. Here, this study aims to elucidate the effects of calcium ions and ROS on tapetal layer development, leading to PCD and subsequent pollen abortion in petalized male-sterile *C. oleifera*. Our results provide important information on the mechanism of male sterility in *C. oleifera*.

2. Materials and Methods

2.1. Plant Materials

The *C. oleifera* cultivar Huashuo (HS) and the petaloid-type male-sterile mutant (HSP) of this variety were eight years old when used as materials in this study. These experimental materials were planted in the Base of Central South University of Forestry and Technology [Pingtang Town, Yuelu District, Changsha City, Hunan Province (112°51′52″ E, 28°02′39″ N)]. The annual average temperature was 19.2 °C, and the soil was low-acid red soil. All plant materials were grown in the experimental field under regular management. Flower buds and anthers of HS and HSP were harvested every two weeks from 10 June 2022 to 15 November 2022, and 50 buds were collected on each occasion. A set of buds and anthers from HS and HSP was sampled and immediately frozen in liquid nitrogen and stored in a −80 °C freezer.

2.2. Morphological Observation of Flower Organs and Pollen Viability

The morphology of the flower organs at the full flowering stage was documented by camera (Nikon D7500, Tokyo, Japan). Mature anthers of HS and HSP were stained with hematoxylin solution (Solarbio, Beijing, China) and treated with methyl salicylate, and then were observed and photographed using an optical microscope (Olympus BX-51, Tokyo, Japan) equipped with a digital camera (Olympus DP73, Tokyo, Japan). Ten anthers were crushed and mixed in 20 mL of distilled water containing Tween-20 and counted in a hemocytometer field to calculate the average number of pollen grains per anther [25]. Pollen viability was examined by an in vitro germination method using 1% (*w*/*v*) agar and 0.01% (*w*/*v*) boric acid. The pollen in the medium was incubated in the oven at 25 °C in darkness for 3 h, and then the number of germination pollen grains was counted under a microscope (Olympus BX51, Tokyo, Japan). The calculation formula was as follows: pollen viability (%) = (germination pollen grains/total pollen grains) × 100. For each repeat, at least three visual regions containing about 50 pollen grains were randomly selected [26].

2.3. Morphological and Cytological Observations

For morphological analysis, a set of flower buds and anthers was removed and then photographed using a stereomicroscope (Olympus SZX-16, Tokyo, Japan) and a camera (Nikon D7500, Tokyo, Japan). Cytological observations of bud and anther development were performed using the paraffin sectioning method. Flower buds with stripped-off scales and anthers at the later stage of development were first fixed in Carnoy's fluid (glacial acetic acid: 95% ethanol at 1:3 *v*/*v*) for 16 h, transferred to a 70% ethanol solution, and stored in a 4 °C refrigerator. Specimens were dehydrated with ethanol, permeated with xylene, embedded with paraffin, and sliced using a microtome (Leica RM2235, Wetzlar, Germany). The thickness of each slice was 8 μm. The slices were stained with hematoxylin and safranin O (Solarbio, Beijing, China), and were finally observed under an optical microscope (Leica DM2500, Wetzlar, Germany) [27]. Another set of materials was fixed in 2.5% glutaraldehyde with 0.1 M phosphate-buffered solution (pH 7) for observations of microspore morphology by transmission electron microscopy (HITACHI7700, Tokyo, Japan) [28].

2.4. Potassium Antimonate Precipitation

In this study, potassium antimonate was used to bind loose calcium, enabling its visualization as black spots under an electron microscope. The selected anthers were fixed in freshly prepared 2.5% (*v*/*v*) glutaraldehyde with 0.1 M phosphate buffer (KH_2PO_4, pH 7.8) containing 1% (*w*/*v*) potassium antimonate ($K_2H_2Sb_2O_7$) for 4 h at room temperature. The glutaraldehyde-fixed samples were washed in five changes (30 min each) with the same buffer, and then postfixed in 1% (*w*/*v*) osmium tetroxide (OsO_4) in the same buffer (0.1 M KH_2PO_4) containing 1% (*w*/*v*) antimonate for 16 h at 4 °C. After OsO_4 fixation, the samples were washed with phosphate buffer without antimonate three times (30 min each), and then dehydrated in a graded acetone series and embedded in Spurr's resin [29]. The samples were sliced to 80 nm ultra-thin sections (cross sections through the anther) with an ultramicrotome, stained with 2.5% (*w*/*v*) uranyl acetate and 0.4% (*w*/*v*) lead citrate solutions, and photographed with a TEM (HITACHI7700, Tokyo, Japan) transmission electron microscope at 80 kV [30,31].

2.5. Determination of H_2O_2 and MDA Content

The H_2O_2 contents of samples were determined using the standard curve method. Fresh anthers from different stages (0.1 g) were ground in acetone into a homogenate and centrifuged at 10,000 rpm at 4 °C for 10 min, according to the instructions of the hydrogen peroxide content detection kit (Solarbio, Beijing, China). A standard solution of 1 mmol/mL hydrogen peroxide treated with the same procedure was used as a control. The absorbance value of the treated samples was measured at 415 nm wavelength, and the hydrogen peroxide content of fresh tissue weight was calculated [32].

For MDA measurement, the samples were mixed and ground in distilled water, a 0.5% (*w*/*v*) thiobarbituric acid solution with 20% trichloroacetic acid was added, and the samples were bathed in water at 100 °C for 10 min. The absorbance was determined at 450 nm, 532 nm, and 600 nm, and MDA content was calculated according to Zhang [32].

2.6. Detection of ROS-Scavenging Enzyme Activities

The detection of SOD, POD, and CAT enzyme activities was performed according to Demircan et al. [33]. First, 0.1 g samples were weighed and ground into powder in liquid nitrogen and homogenized in 500 µL buffer (50 mM Tris-HCl, 1% (*w*/*v*) PVP, 0.1% (*w*/*v*) Triton X-1000, 1 mM EDTA) for enzyme extraction. After centrifuging the supernatant at 4 °C for 10 min (12,000 rpm), the supernatants were treated with SOD, POD, and CAT detection kits (Solarbio, Beijing, China), and the absorbances were measured at 560 nm, 470 nm, and 240 nm, respectively. The enzyme activity was calculated according to the manufacturer's instructions.

2.7. Expression Analyses via RT-qPCR

A Plant RNA Extraction Kit (Omega, Beijing, China) was used to extract total RNA from the different anther developmental stages, and first-strand cDNA for the RT-qPCR was synthesized according to the instructions of HiScript II Q RT SuperMix (Vazyme, Nanjing, China). The total volume of the qPCR reaction system was 20 µL, including 10 µL of 2 × ChamQ Universal SYBR qPCR Master Mix (Vazyme, Nanjing, China), each with 0.5µmol/L of forward and reverse primers, 1µL of ten-fold diluted cDNA template, and 8µL ddH2O. The PCR conditions were as follows: denaturation at 95 °C for 30 s; 40 cycles of denaturation at 95 °C for 10 s; and annealing and extension at 60 °C for 30 s. Gene expression was calculated using the $2^{-\Delta\Delta Ct}$ method. The house-keeping gene *GAPDH* was used as an internal control for normalization [34]. These selected gene sequences were based on the genome of *C. oleifera* [35]. The primer sequences of the reference gene (*GAPDH*) and of selected genes are shown in Supplemental Table S1.

2.8. Statistical Analysis

Data analyses were performed using Excel 2010 and SPSS 17.0 software (SPSS, Chicago, IL, USA). Data, presented as mean ± SD, were obtained from three replicates. $p < 0.05$ was considered statistically significant, and $p < 0.01$ was considered extremely significant.

3. Results

3.1. Morphological Analysis of Flower Organs of HS and HSP

There were significant differences in anther morphology between HS and HSP (Figure 1). The anthers of HSP had no pollen sacs and became completely petal-like, with traces of degenerated pollen sacs and abortive pollen grains (Figure 1E,F). HSP anthers hardly produced pollen and the pollen germination rate was almost 0, while HS anthers had more pollen grains (2682 ± 431 per anther) with a pollen vigor of 61.16% (Figure 1G,H).

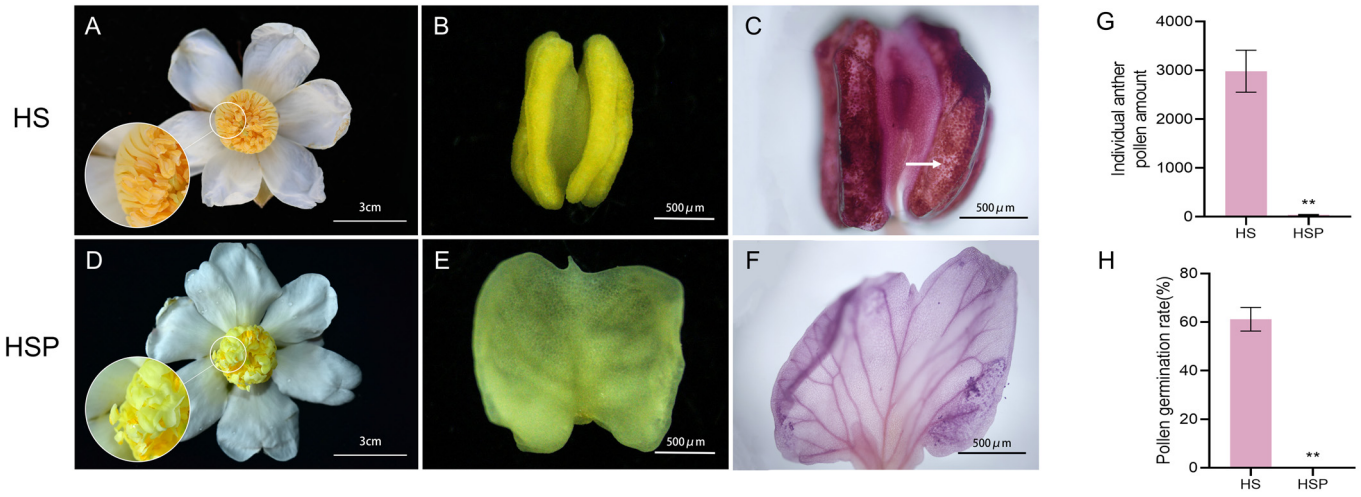


Figure 1. Comparison of flower organ morphologies and pollen viability between HS and HSP anthers of *Camellia oleifera*. (**A**–**C**) Flower and normal anther morphology of fertile plants (HS). (**D**–**F**) Flower and petalized anther morphology of petaloid-type male-sterile mutant (HSP). (**G**) Individual anther pollen amount of *C. oleifera* plants (HS and HSP). (**H**) Pollen germination rates of *C. oleifera* plants (HS and HSP). The arrows point to the pollen grain. Values are means ± SD of 3 replicates. Asterisks represent statistically significant differences between HSP and HS (Student's *t*-test ** $p < 0.01$).

3.2. Cytological Characterization of Anther Development

Based on microscopic observations, we divided HS and HSP anther development into 10 stages (Figure 2A,B). In S1–S2, HS and HSP gradually formed anthers and filaments from stamen primordia (Figure 2A(VII,XVII)). At S3, anthers underwent differentiation localized on the corners to form four pollen sacs (Figure 2A(VIII,XVIII)). From S4 to S5, the anther size increased, the morphology gradually completed, and four complete pollen sacs formed completely (Figure 2A). At S6 (secondary sporogenous cell stage), concentrically arranged outside the secondary sporogenous cells were five layers of cells: the epidermis, the endothecium, two middle layers, and the tapetum (Figure 2B(VI,XVI)). There was no significant difference in S1–S6 between sterile HSP and fertile HSP.

At S7 (microspore mother cell stage), a single callose-coated microspore mother cell began meiosis, the tapetum cells enlarged, the layer thickness increased, and the color deepened (Figure 2B(VII)). Contrastingly, the tapetal layer of HSP anthers was obviously abnormal, and tapetal cells were seriously vacuolated and their color was lighter, showing an obvious degradation trend (Figure 2B(XVII)). At S8 (tetrad stage), the microspore mother cells in HS successfully produced tetrads, and the tapetum cells were neatly arranged and dark in color. On the contrary, no typical tetrads were observed in mutant HSP, and the residual tapetum cells were uneven in shape with a collapsed anther wall (Figure 2B(VIII,XVIII)). With the degradation of the tapetum, the free microspore gradually

developed into mature pollen grains. At S9, the pollen grains in HS anthers were more strongly stained. Only the epidermis, endothecium, and a few middle layer cells remained in the anther wall, the endothecium layer was obviously thickened, and the tapetum cells had completely disappeared (Figure 2B(IX)). The HSP anther compartment collapsed inward and an abnormal vascular bundle development was observed. In the abortive anthers, only a small proportion of mature pollen grains was observed, and the area of pollen sacs had gradually shrunk, eventually forming flat petal-like structures (Figure 2B(XIX)). Finally, at S10, or the flowering stage, the HS anthers cracked open normally and released pollen (Figure 2B(X)). On the other hand, no mature pollen grains were observed in the squeezed residual anthers of HSP (Figure 2B(XX)).

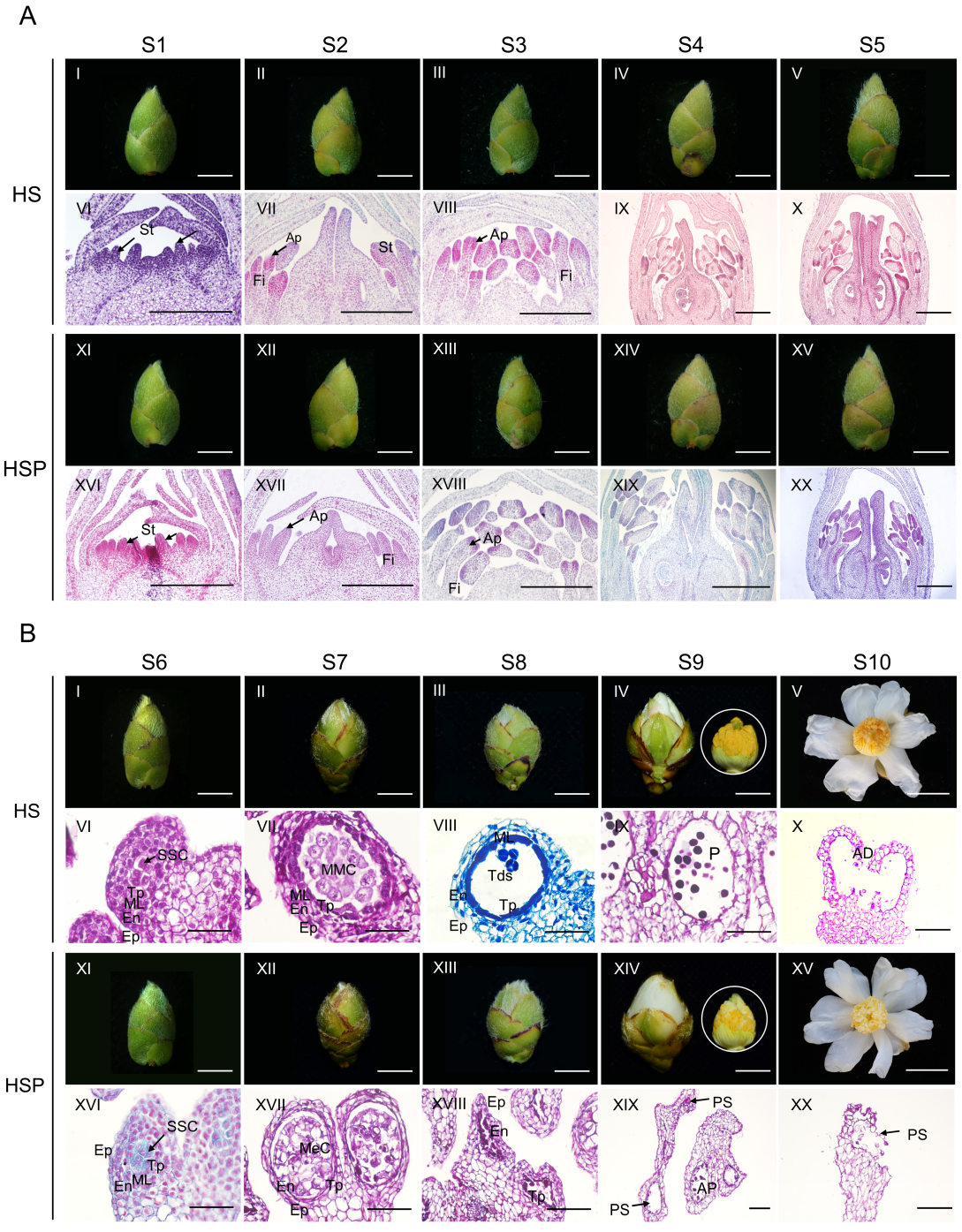


Figure 2. Anther development stage of the male fertile *Camellia oleifera* HS and the male-sterile plant HSP. (**A**) Anther development of HS and HSP during stages 1 to 5. (**B**) Anther development of HS

and HSP during stages 6 to 10. (**A**,**B**(**I–V**,**XI–XV**)) External morphology of the flower buds of HS and HSP. (**A**(**VI**,**XVI**)) Longitudinal elongation of stamen primordium between HS and HSP. (**A**(**VII**,**VIII**,**XVII**,**XVIII**)) Differentiation of anthers and filaments between HS and HSP. (**A**(**IX**,**X**,**XIX**,**XX**)) Anthers develop further to form pollen sacs of HS and HSP. (**B**(**VI**,**XVI**)) The differentiation of primary sporogenous cells of HS and HSP produced secondary sporogenous cells. (**B**(**VII**,**XVII**)) Microspore mother cells undergo meiosis of HS and HSP. (**B**(**VIII**)) The microspore mother cells of HS formed tetrads. (**B**(**XVIII**)) The tapetum was degraded seriously, and the anther wall collapsed inward, and no tetrad was formed in HSP. (**B**(**IX**)) The microspores matured, the tapetum and middle layers were already degraded in HS. (**B**(**XIX**)) Petalized anthers contain only residual pollen sacs in HSP. (**B**(**X**)) The anthers cracked to release pollen in HS. (**B**(**XX**)) Pollen sac traces of abortion in HSP. St, stamen; Ap, anther primordium; Fi, filament; Ep, epidermis; PSC, primary sporogenous cell; SSC, secondary sporogenous cell; En, endothecium; ML, middle layer; Tp, tapetum; MMC, microspore mother cell; Tds, tetrads; P, pollen; AP, abortive pollen; MeC, meiotic cell; AD, anther dehiscence; PS, pollen sacs. Scale bars: 5 mm (**A**(**I–V**,**XI–XV**),**B**(**I–IV**,**XI–XIV**)); 3 cm (**B**(**V**,**XV**)); 200 μm (**A**(**VI–X**,**XVI–XX**)); 50 μm (**B**(**VI–X**,**XVI–XX**)).

3.3. Ultrastructure Observation of Early Anther Development

During the sporogenous cell stage, both HS and HSP anthers developed primary sporogenous cells and primary wall cells (Figure 3A–D). At S6, the five-layer wall cells of HS were arranged neatly, while the secondary sporogenous cells of HSP had an uneven cytoplasm and signs of vacuolation (Figure 3E–H). Upon entering the microspore mother cell stage at S7, the cell arrangement of microspore mother cells became looser compared to sporogenous cells, featuring more intercellular spaces and callose formation. Microspore mother cells also produced more plastids with low electron density and small starch particles (Figure 3I–L). After meiosis, the four haploid spores produced by HS were encased in callose, while the callose wall of HSP showed signs of irregular shrinkage. The anther wall cells did not change significantly from the previous stage, and the innermost tapetum cells were more tightly packed than before, and their shape was more irregular. These cells contained many small organelles, with a large number of mitochondria in particular and scattered fragments of the endoplasmic reticulum contained in the tapetum (Figure 3M–P).

3.4. Distribution of Calcium Ions in HS and HSP Anthers during S8–S10

Compared to tetrad cells, early microspores exhibited more calcium precipitates, initially located within the cell nucleus. During development, several large vacuoles appeared in the microspores, and their cell nuclei migrated to the cell peripheries. Throughout this process, the amount of calcium precipitates in HS increased overall, significantly more than in HSP. The tapetal layer cells of both HS and HSP increased in size, displaying a trend of degradation, and becoming discontinuous and irregularly wrinkled in appearance (S8–1) (Figure 4A1–A8). In late S8 (S8–2), the degradation of the tapetal layer in HSP was notably higher than in HS, with a large amount of calcium ion precipitation in the cells. Granular substances appeared on the tangential surfaces of the HS tapetal layer cells, likely representing the Ubisch bodies involved in the synthesis of pollen exine. In contrast, the degradation of HSP tapetal layer cells was more pronounced, with Ubisch bodies unevenly distributed in the cytoplasm after the breakdown of the tapetal layer. At this stage, the epidermal cells, endothelial cells, and middle layer cells showed no significant changes and maintained a high degree of vacuolization (Figure 4A9–A16). In the late stages of microspore development in S9, large vacuoles appeared, occupying the central region of the cells, and the cell nucleus and cytoplasm were pushed towards the periphery, indicating the mononucleate stage of pollen. The structure of tapetal layer cells in HS and HSP anther walls disappeared at this stage, with the Ca content degrading. During this period, the deposition of calcium in HSP was more than that in HS (Figure 4A17–A24). The mature anther wall consisted of three layers of cells: the outermost layer or epidermis, the middle layer with a noticeable radial thickening of the wall, and the innermost layer consisting of middle layer cells. The tapetum and middle layers of HS were already degraded, and

the endothecium radially thickened, while the anther wall cells of HSP transformed into parenchyma cells similar to petal cells. In the mature pollen of S10, there were no calcium precipitates in the cytoplasm; instead, they accumulated at the pollen wall. The ornamentation of the outer wall of HSP pollen was irregular, and the pollen wall was thicker compared to HS, where the pollen cell wall was denser (Figure 4A25–A32).

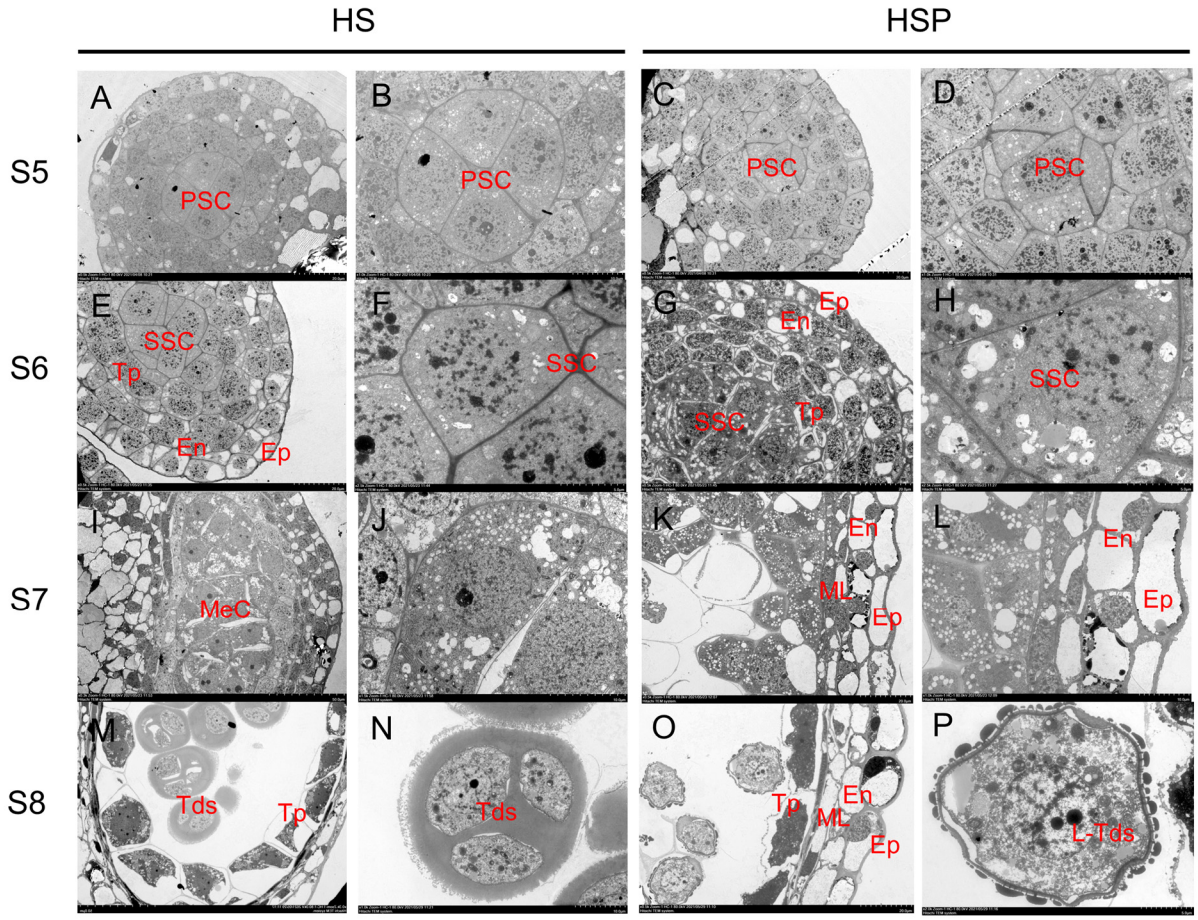


Figure 3. Ultrastructure observations of anther wall and pollen in HS and HSP from stages 5 to 8 using transmission electron microscopy (TEM). (**A**–**D**) The primary sporogenous cells of HS and HSP began mitosis. (**E**–**H**) The differentiation of primary sporogenous cells of HS and HSP produced secondary sporogenous cells. (**I**–**L**) Five layers of anther parietal cells were formed in HS and HSP, which were the epidermis (one layer), endothecium (one layer), middle layer (two layers), and tapetum layer (one layer) from the outside to inside, respectively. Individual microspore mother cells undergo meiosis (**M**,**N**) The tetrad cells of HS were uniformly encased in callose. (**O**,**P**) The tetrad callose of HSP underwent degradation. Ep, epidermis; PSC, primary sporogenous cell; SSC, secondary sporogenous cell; En, endothecium; ML, middle layer; Tp, tapetum; MMC, microspore mother cell; MeC, meiotic cell; Tds, tetrads; L-Tds, late tetrads.

3.5. Accumulation of ROS in HS and HSP

The H_2O_2 content in HS and HSP continuously increased in the early anther developmental stages, with an overall trend of first increasing and then decreasing. The H_2O_2 content in HSP began to be significantly higher than HS at S6, peaking at 23.78 $\mu mol \cdot g^{-1}$ at S7, equivalent to 71.82% greater than the HS control, and HSP remained higher at S6–S9 (Figure 5A). Compared with HS, the MDA content in HSP was higher in the late anther development stages, with the content at S8 significantly higher, reaching 6.94 $\mu mol \cdot g^{-1}$, corresponding to a significant increase of 84.57% compared with HS (Figure 5B).

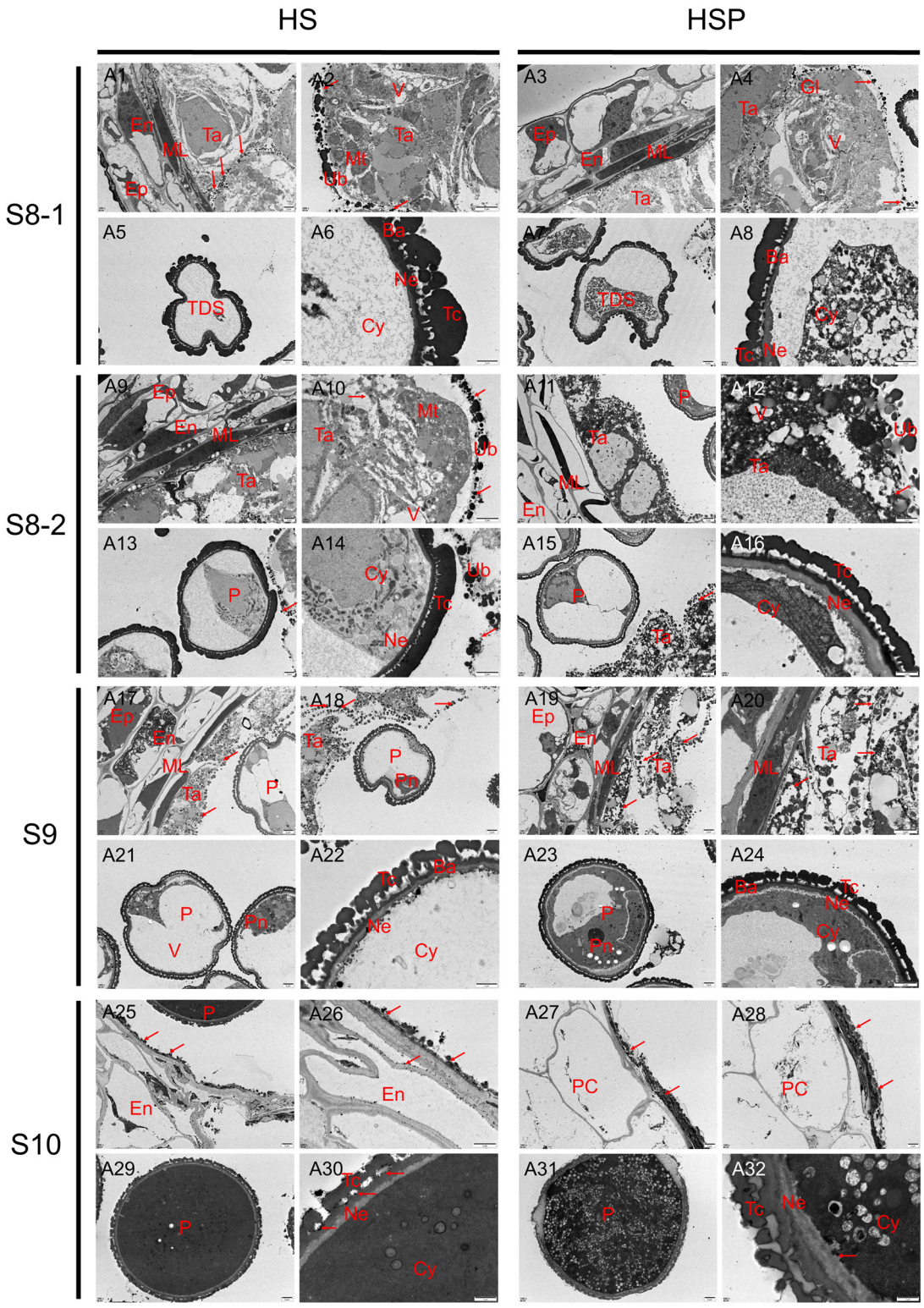


Figure 4. Distribution of calcium precipitates bound by potassium antimonate in the anthers of HS and HSP during S8–S10. (**A1**–**A8**) Comparison of tapetal cells and microspores morphology between HS and HSP at tetrad stage (S8–1), Calcium ions deposited in the inner side of tapetal cells formed a deposition zone in HS. (**A9**–**A16**) Comparison of tapetal cells and microspores morphology between HS and HSP at late tetrad stage (S8–2), the degradation of HSP tapetal cells was more obvious, and the distribution of Ca^{2+} in the cytoplasm was uneven after degradation of tapetum. (**A17**–**A24**) In the late stage of microspore development (S9), the cell structure of tapetal layer of anther wall of HS and

HSP disappeared, and calcium deposition in HSP was more than that in HS. (**A25**–**A32**) In mature anthers (S10), the middle layers of HS were degenerated and the tapetal cells were completely gone, and calcium deposits accumulate in pollen walls. The anther wall cells of HSP transformed into parenchyma cells similar to petal cells. Ep, epidermis; En, endothecium; ML, middle layer; Ta, tapetum; Tds, tetrads; P, pollen; V, vacuole; Mt, mitochondrion; Ub, Ubisch body; Gl, golgiosome; Tc, tectum; Ne, nexine; Ba, bacula; Cy, cytoplasm; PC, parenchymal cell. The arrows point to the calcium precipitation.

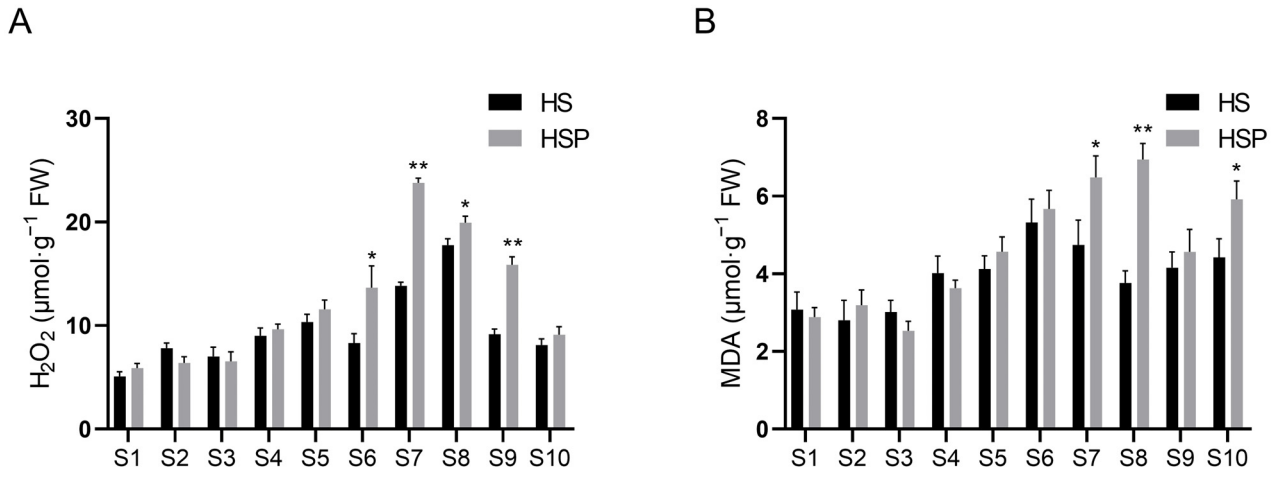


Figure 5. Accumulation of H_2O_2 and MDA in the anthers of HS and HSP during various developmental stages. (**A**) H_2O_2 content; (**B**) MDA content. Values are means ± SD of 3 replicates. Asterisks represent statistically significant differences between HSP and HS (Student's *t*-test * $p < 0.05$, ** $p < 0.01$).

3.6. Enzymatic Activities of ROS Scavenging

The POD activity of HSP anthers was always lower than that of HS at the different developmental stages, and the POD activity of HS had a significant peak in S8, reaching 20.13 U·g^{-1} FW·min^{-1}, which was twice that of HSP (Figure 6A). Compared to HS, SOD activity was significantly lower than HS only in the tetrad stage (S8), and there were no significant differences in the other stages (Figure 6B). For HSP, CAT activity decreased significantly in stages 7 to 8, corresponding to 30.66% and 30.06% lower than the control, respectively, but increased significantly at S9 (Figure 6C). The difference in antioxidant enzyme activity between HS and HSP was mainly focused in S7–S8, which is the critical period of microspore abortion and tapetum degradation.

3.7. Expression Analysis of Related Genes

CoNADPH was higher in the early stages of pollen development (S7–S8) but lower in the tetrad to pollen maturity stages; however, these differences were not significantly different between HS and HSP. *CoPOD* was upregulated with pollen development, and POD expression in HSP was lower than that in HS. The expression of *CoCAT* increased gradually in S6–S8 of HS and HSP, and was lower in the anthers of HSP than those of HS (48.38% and 44.52% in S7 and S8 stages, respectively), and yet had no significant difference in S9–S10. The expression of the *CoCPK* gene in HSP anthers was higher in S7 and S8, reaching 3.10 times and 1.77 times that of HS, respectively (Figure 7). In contrast, calmodulin *CoCaM1* and *CoCaM2* expressed more HS than HSP during this period.

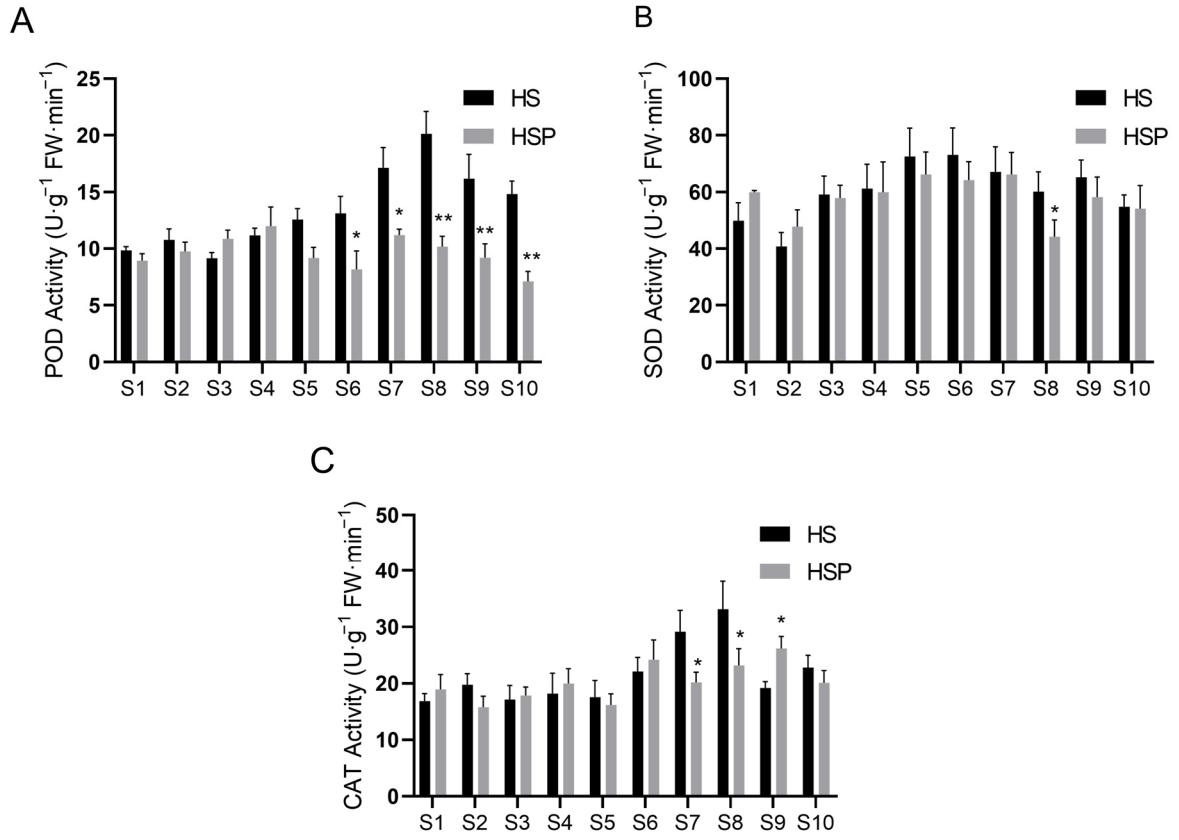


Figure 6. Determination of POD (**A**), SOD (**B**) and CAT (**C**) activities in the anthers of HS and HSP during various developmental stages. Values are means ± SD of 3 replicates. Asterisks represent statistically significant differences between HSP and HS (Student's *t*-test * $p < 0.05$, ** $p < 0.01$). POD, peroxidase; SOD, superoxide dismutase; CAT, catalase.

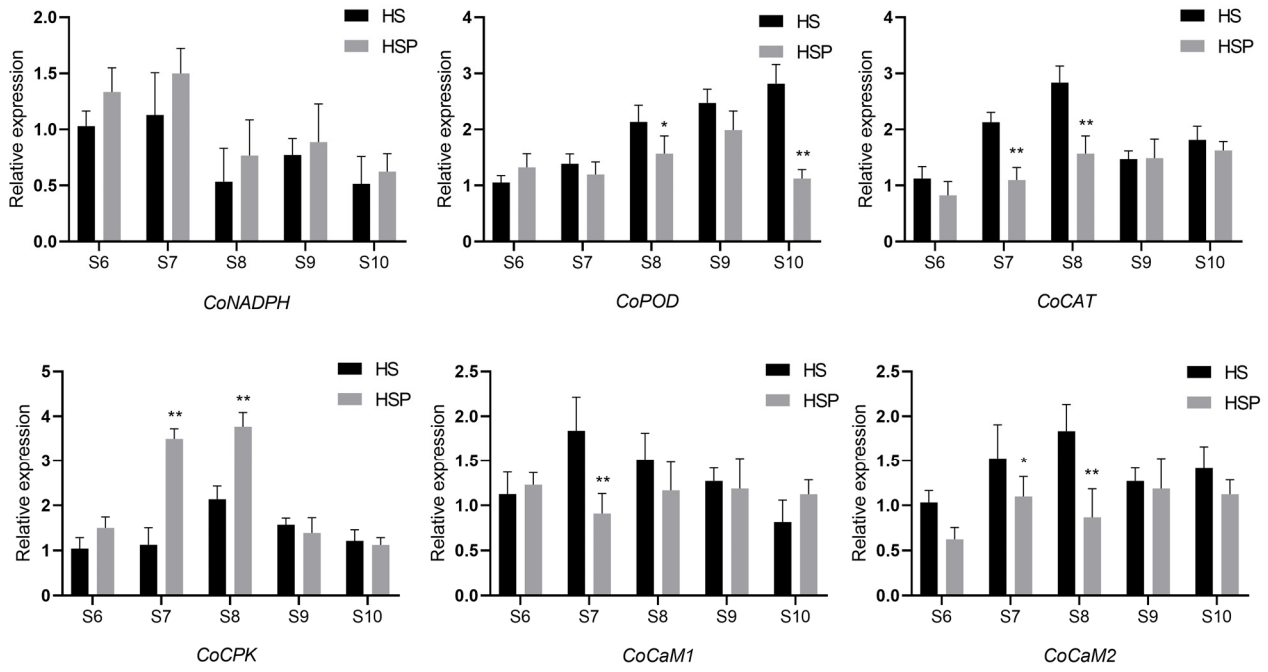


Figure 7. Results of gene expression for related genes in the anthers of HS and HSP during pollen developmental stages. Values are means ± SD of 3 replicates (Student's *t*-test * $p < 0.05$, ** $p < 0.01$).

4. Discussion

4.1. The Critical Period of Abortion and Tapetum PCD in CMS HSP Plant

The CMS mechanism is completely different in different plants. To date, four models have been proposed to explain the CMS mechanism, namely, the cytotoxicity model, the energy deficit model, the retrograde regulation model, and the abnormal programmed cell death (PCD) model [7]. The investigation of key periods during anther development is crucial for unraveling the specific CMS mechanism of HSP. In dicotyledonous plants, most miscarriages occur during the tetrad and microspore development stages. In seedless 'Ougan' mandarin (*Citrus suavissima*), the pollen miscarriage of anthers occurred during the tetrad stage of microspore development, and functional pollen failed to develop [36,37]. In the male-sterile mutant Se18 of watermelon, microsporocytes were blocked from meiosis and defective tapetum cells produced multiple layers of tapetum [38]. In this report, we observed significant differences between the male-sterile mutant HSP and the male fertile HS at the microspore mother cell stage (S7). The abnormal development of microspore mother cells coincided with the premature degradation of the tapetal layer. A similar result was reported in maize (*Zea mays*) male-sterile line ms39, where the premature PCD of tapetum layer cells in anthers led to anther wall structural collapse [17]. The anther tapetum layer provides essential nutrients for microspore development, and the timely degradation of the tapetum layer is crucial for pollen grain development [39]. The tapetal cells of HSP had abnormal organelle fragmentation at S7, and premature PCD in the tapetal layer disrupted energy metabolism, which eventually led to pollen abortion. Similar results were reported in *Actinidia deliciosa* [40] and *Tillandsia albida* [41].

4.2. Abnormal ROS and Antioxidant Defense System Leading to Tapetum PCD

The production of ROS is an important factor in plant PCD signaling male sterility in plants [42]. The presence of excess ROS in wheat was associated with abnormal PCD progression in the tapetal layer [43]. An abnormal accumulation of ROS was also found in kenaf CMS line P9SA [44]. MDA is a common indicator of peroxidation related to oxidative stress, and usually high MDA can cause cell damage through nucleic acid reaction with proteins, lipids, and organelles [45]. In our study, the H_2O_2 content and MDA content of HSP were significantly higher in S7–S8, showing consistency with the abnormal PCD stage of the tapetum. Thus, we propose that excess ROS may be the main factor leading to premature PCD in the tapetum. Similar ROS-induced PCD has been described in *Olea europaea* [46].

SOD, POD, and CAT are considered as key antioxidant enzymes that can eliminate excess ROS [18]. In our study, the POD activity of anthers in HSP was always lower than that in HS during the pollen development stage, and SOD activity and CAT in the tetrad stage were also significantly lower than that in HS. In fact, the lack of antioxidant system in HSP led to the overproduction of ROS, thus upsetting the ROS balance. In cotton CMS line Jin A, the activity of POD and CAT in anthers was significantly reduced, and excess ROS was produced [32]. The soybean CMS line SXCMS5A also reported the same results with reduced anther ROS scavenging [47].

The activity of antioxidant enzymes in anthers is regulated by related genes. In the YamianA line in cotton, the expression trend of *MnSOD* was the same as SOD activity and the expression trend of CAT1 was the same as CAT [32]. In our study, the expression levels of *CoPOD* and *CoCAT* genes were uniformly upregulated in the early stage of HSP pollen development, but were lower than that in HS at the same stage, which was similar to the trend of enzyme activity. ROS production was associated with the stage-specific expression of NADPH oxidase [48]; however, the *CoNADPH* gene did not show regular fluctuations in this study, suggesting that the source of excess ROS in HSP pollen was not NADPH oxidase. Disorder at the enzyme gene transcription level may be closely related to ROS production, and the antioxidant system cannot effectively eliminate the excessive production of ROS, resulting in the long-term oxidative stress of microspores during anther development. Similar results have been reported in a novel CMS line SaNa-1A of *B. napus*,

in which an excessive accumulation of ROS and lack of an antioxidant enzyme system affected anther development [15].

4.3. Calcium Distribution and Function during the Anther Development

Previous studies have shown that one of the causes of male sterility is excessive Ca^{2+} concentration in anthers [21]. In PGMR sterile anthers in rice, calcium precipitates were abundant in the endothecium and middle layer, but less distributed in the tapetal cells [21]. In a CMS line of purple rice from Yunnan, a large number of calcium ion particles appeared between the tapetum and microspore, but less calcium ions appeared in the tapetum cells [49]. In this study, we analyzed the distribution of calcium ions after a period of difference between HS and HSP; the tapetal layer of HSP was degraded earlier than that of HS at the tetrad stage, and the calcium precipitation of the anther tapetal layer of HSP was less than that of HS. In HS anthers, calcium precipitates were uniformly distributed on the inner part of the tapetum near the callose wall, and were widely distributed on the middle cell wall, while HSP was unevenly distributed near the tapetum organelles. These characteristics were similar to the results of abnormal calcium ions in the tapetum layer of sterile anthers in rice [49]. After microspores were released from the tetrad, calcium appeared between the endexine and intine at pollen maturity, which was also found in previous studies [29]. The accumulation of calcium in the callose wall of the tapetum and tetrad related to the formation of the pollen wall, similar to the way that the tapetum provides nutrients and metabolites for anthers, and there was a migration of tapetum calcium to the pollen wall [50]. Thus, the abnormal distribution of calcium ions in HSP may participate in the process of microspore abortion.

Cellular calcium homeostasis depends on Ca^{2+}-ATPase and the expression of related genes. It has been reported that Ca^{2+}-dependent kinase 5 can promote ROS production by inhibiting the activity of *CPK5*-mediated catalase protein *CAT1* [24]. Our results show that *CoCPK* was highly expressed in early pollen development. The expression of HSP in the S7–S8 period was significantly higher than that of HS, which was similar to the change in the trend of ROS physiological indexes, indicating that calcium ions and reactive oxygen species may co-mediate the tapetal PCD of anthers in early pollen development.

5. Conclusions

Cytological analysis indicated that the main cause of HSP abortion was the premature PCD of the tapetum layer at the tetrad stage. Our research highlights the significant role of ROS and the antioxidant defense system in tapetum PCD, with HSP exhibiting disrupted antioxidant enzyme activities compared to the control. The overaccumulation of ROS and the deficiency in the antioxidant enzyme system induced premature PCD in the tapetum, thereby affecting pollen development. Furthermore, we explored the distribution and function of calcium ions during anther development, uncovering irregular calcium distribution in HSP pollen walls. These results suggest a potential co-mediation of tapetal PCD by calcium ions and ROS, and provide valuable insights into the molecular and physiological mechanisms of male sterility in CMS plants with petaloid anthers. Further exploration of the molecular biological mechanisms regulating CMS is essential to realize its application in the field of breeding.

Supplementary Materials: The following supporting information can be downloaded at: https://www.mdpi.com/article/10.3390/agronomy14030585/s1, Table S1: List of primer sequences of selected genes.

Author Contributions: Conceptualization, X.G. and Y.Y.; methodology, X.G., Y.Y. and J.Y.; validation, D.Y. and H.X.; formal analysis, X.G.; investigation, D.Y. and H.X.; writing—original draft preparation, X.G.; writing—review and editing, F.Z.; visualization, X.G. and F.Z. All authors have read and agreed to the published version of the manuscript.

Funding: The project was partly supported by the National Natural Science Foundation of China (No. 32271841), the National Key R&D Program of China (Grant No. 2022YFD2200400), and the Hunan Provincial Natural Science Foundation of China (No. 2021JJ31157).

Data Availability Statement: The data presented in this study are available on request from the corresponding author. The data are not publicly available due to privacy.

Conflicts of Interest: The authors declare no conflicts of interest.

References

1. Gao, D.-F.; Xu, M.; Zhao, P.; Zhang, X.-Y.; Wang, Y.-F.; Yang, C.-R.; Zhang, Y.-J. Kaempferol Acetylated Glycosides from the Seed Cake of *Camellia oleifera*. *Food Chem.* **2011**, *124*, 432–436. [CrossRef]
2. Luan, F.; Zeng, J.; Yang, Y.; He, X.; Wang, B.; Gao, Y.; Zeng, N. Recent Advances in *Camellia oleifera* Abel: A Review of Nutritional Constituents, Biofunctional Properties, and Potential Industrial Applications. *J. Funct. Foods* **2020**, *75*, 104242. [CrossRef]
3. Huang, L.; Tan, X.; Long, H.; Jiang, N. An Analysis and Research on Biosynthesis Pathway and Gene Regulation of Fatty Acid of *Camellia oleifera* Seeds. *J. Chem. Pharm. Res.* **2013**, *5*, 1252–1257.
4. Song, Q.; Gong, W.; Yu, X.; Ji, K.; Chang, Y.; Wang, L.; Yuan, D. Integrative Analysis of the Metabolome and Transcriptome Provides Novel Insights into the Mechanisms of Flavonoid Biosynthesis in *Camellia lanceoleosa*. *Sci. Hortic.* **2022**, *304*, 111357. [CrossRef]
5. Yuan, L. Progress in Super-Hybrid Rice Breeding. *Crop J.* **2017**, *5*, 100–102. [CrossRef]
6. Chen, X.; Zhang, H.; Sun, H.; Luo, H.; Zhao, L.; Dong, Z.; Yan, S.; Zhao, C.; Liu, R.; Xu, C.; et al. IRREGULAR POLLEN EXINE1 Is a Novel Factor in Anther Cuticle and Pollen Exine Formation. *Plant Physiol.* **2017**, *173*, 307–325. [CrossRef]
7. Chen, L.; Liu, Y.-G. Male Sterility and Fertility Restoration in Crops. *Annu. Rev. Plant Biol.* **2014**, *65*, 579–606. [CrossRef]
8. Kozik, E.U.; Nowak, R.; Nowakowska, M.; Dyki, B. Level of Sterility and Morphological Flowers Differentiation of Petaloid Male-Sterile Plants of Carrot. *J. Agric. Sci.* **2012**, *4*, 187. [CrossRef]
9. Yu, X.; Lu, H.; Lu, G.; Chen, Z.; Cao, J.; Hirata, Y. Analysis of Genetic Diversity in Cytoplasmic Male Sterility, and Association of Mitochondrial Genes with Petaloid-Type Cytoplasmic Male Sterility in Tuber Mustard (*Brassica juncea* Var. Tumida Tsen et Lee). *Mol. Biol. Rep.* **2010**, *37*, 1059–1067. [CrossRef] [PubMed]
10. Xiong, H.; Chen, P.; Zhu, Z.; Chen, Y.; Zou, F.; Yuan, D. Morphological and Cytological Characterization of Petaloid-Type Cytoplasmic Male Sterility in *Camellia oleifera*. *HortScience* **2019**, *54*, 1149–1155. [CrossRef]
11. Hu, Y.; Gao, C.; Deng, Q.; Qiu, J.; Wei, H.; Yang, L.; Xie, J.; Liao, D. Anatomical Characteristics of Petalized Anther Abortion in Male Sterile *Camellia oleifera* Plants. *J. Am. Soc. Hortic. Sci.* **2021**, *146*, 411–423. [CrossRef]
12. Liu, B.; Ou, C.; Chen, S.; Cao, Q.; Zhao, Z.; Miao, Z.; Kong, X.; Zhuang, F. Differentially Expressed Genes between Carrot Petaloid Cytoplasmic Male Sterile and Maintainer during Floral Development. *Sci. Rep.* **2019**, *9*, 17384. [CrossRef] [PubMed]
13. Heng, S.; Gao, J.; Wei, C.; Chen, F.; Li, X.; Wen, J.; Yi, B.; Ma, C.; Tu, J.; Fu, T.; et al. Transcript Levels of Orf288 Are Associated with the Hau Cytoplasmic Male Sterility System and Altered Nuclear Gene Expression in *Brassica juncea*. *J. Exp. Bot.* **2018**, *69*, 455–466. [CrossRef] [PubMed]
14. Heng, S.; Chen, F.; Wei, C.; Li, X.; Yi, B.; Ma, C.; Tu, J.; Shen, J.; Fu, T.; Wen, J. Cytological and iTRAQ-Based Quantitative Proteomic Analyses of Hau CMS in *Brassica napus* L. *J. Proteom.* **2019**, *193*, 230–238. [CrossRef] [PubMed]
15. Du, K.; Xiao, Y.; Liu, Q.; Wu, X.; Jiang, J.; Wu, J.; Fang, Y.; Xiang, Y.; Wang, Y. Abnormal Tapetum Development and Energy Metabolism Associated with Sterility in SaNa-1A CMS of *Brassica napus* L. *Plant Cell Rep.* **2019**, *38*, 545–558. [CrossRef] [PubMed]
16. Li, Z.; Zhu, T.; Liu, S.; Jiang, Y.; Liu, H.; Zhang, Y.; Xie, K.; Li, J.; An, X.; Wan, X. Genome-Wide Analyses on Transcription Factors and Their Potential microRNA Regulators Involved in Maize Male Fertility. *Crop J.* **2021**, *9*, 1248–1262. [CrossRef]
17. Niu, Q.; Shi, Z.; Zhang, P.; Su, S.; Jiang, B.; Liu, X.; Zhao, Z.; Zhang, S.; Huang, Q.; Li, C.; et al. ZmMS39 Encodes a Callose Synthase Essential for Male Fertility in Maize (*Zea mays* L.). *Crop J.* **2023**, *11*, 394–404. [CrossRef]
18. Wang, S.; Zhang, G.; Song, Q.; Zhang, Y.; Li, Y.; Guo, J.; Chen, Z.; Niu, N.; Ma, S.; Wang, J. Programmed Cell Death, Antioxidant Response and Oxidative Stress in Wheat Flag Leaves Induced by Chemical Hybridization Agent SQ-1. *J. Integr. Agric.* **2016**, *15*, 76–86. [CrossRef]
19. Zhou, B.; Liu, Y.; Chen, Z.; Liu, D.; Wang, Y.; Zheng, J.; Liao, X.; Zhou, R. Comparative Transcriptome Analysis Reveals the Cause for Accumulation of Reactive Oxygen Species During Pollen Abortion in Cytoplasmic Male-Sterile Kenaf Line 722HA. *Int. J. Mol. Sci.* **2019**, *20*, 5515. [CrossRef]
20. Ma, L.; Hao, Y.; Liu, X.; Shao, L.; Wang, H.; Zhou, H.; Zhang, D.; Zhu, T.; Ding, Q.; Ma, L. Proteomic and Phosphoproteomic Analyses Reveal a Complex Network Regulating Pollen Abortion and Potential Candidate Proteins in TCMS Wheat. *Int. J. Mol. Sci.* **2022**, *23*, 6428. [CrossRef]
21. Tian, H.Q.; Kuang, A.; Musgrave, M.E.; Russell, S.D. Calcium Distribution in Fertile and Sterile Anthers of a Photoperiod-Sensitive Genic Male-Sterile Rice. *Planta* **1998**, *204*, 183–192. [CrossRef]
22. Batistič, O.; Kudla, J. Analysis of Calcium Signaling Pathways in Plants. *Biochim. Biophys. Acta (BBA) Gen. Subj.* **2012**, *1820*, 1283–1293. [CrossRef] [PubMed]
23. Verma, S.; Negi, N.P.; Narwal, P.; Kumari, P.; Kisku, A.V.; Gahlot, P.; Mittal, N.; Kumar, D. Calcium Signaling in Coordinating Plant Development, Circadian Oscillations and Environmental Stress Responses in Plants. *Environ. Exp. Bot.* **2022**, *201*, 104935. [CrossRef]

24. Yang, J.; Chen, L.; Zhang, J.; Liu, P.; Chen, M.; Chen, Z.; Zhong, K.; Liu, J.; Chen, J.; Yang, J. TaTHI2 Interacts with Ca^{2+}-Dependent Protein Kinase TaCPK5 to Suppress Virus Infection by Regulating ROS Accumulation. *Plant Biotechnol. J.* **2023**, *early view*. [CrossRef]
25. Chen, C.L.; Guo, W.W.; Yi, H.L.; Deng, X.X. Cytogenetic Analysis of Two Interspecific *Citrus* Allotetraploid Somatic Hybrids and Their Diploid Fusion Parents. *Plant Breed.* **2004**, *123*, 332–337. [CrossRef]
26. Xiong, H.; Zou, F.; Yuan, D.; Zhang, X.; Tan, X. Orthogonal Test Design for Optimising the Culture Medium for in Vitro Pollen Germination of Feijoa (*Acca sellowiana* Cv. Unique). *N. Z. J. Crop Hortic. Sci.* **2016**, *44*, 192–202. [CrossRef]
27. Zou, F.; Chen, S.-L.; Yuan, D.-Y.; Zhang, R.-Q.; Zhang, L.; Xiong, H. Microsporogenesis, Megasporogensis and Male and Female Gametophyte Development in *Feijoa sellowiana* (Myrtaceae). *Int. J. Agric. Biol.* **2016**, *18*, 637–642. [CrossRef]
28. Gao, C.; Yang, R.; Yuan, D. Structural Characteristics of the Mature Embryo Sac of *Camellia oleifera*. *Nord. J. Bot.* **2018**, *36*, njb-01673. [CrossRef]
29. Wei, D.; Gao, C.; Yuan, D. Calcium Distribution during Anther Development in Oil Tea (*Camellia oleifera* Abel.). *J. Am. Soc. Hortic. Sci.* **2015**, *140*, 88–93. [CrossRef]
30. Bednarska, E.; Lenartowska, M.; Niekraś, L. Localization of Pectins and Ca^{2+} Ions in Unpollinated and Pollinated Wet (*Petunia hybrida* Hort.) and Dry (*Haemanthus albiflos* L.) Stigma. *Folia Histochem. Cytobiol.* **2005**, *43*, 249–259.
31. Suwińska, A.; Wasąg, P.; Bednarska-Kozakiewicz, E.; Lenartowska, M.; Lenartowski, R. Calreticulin Expression and Localization in Relation to Exchangeable Ca^{2+} during Pollen Development in Petunia. *BMC Plant Biol.* **2022**, *22*, 24. [CrossRef]
32. Zhang, J.; Zhang, L.; Liang, D.; Yang, Y.; Geng, B.; Jing, P.; Qu, Y.; Huang, J. ROS Accumulation-Induced Tapetal PCD Timing Changes Leads to Microspore Abortion in Cotton CMS Lines. *BMC Plant Biol.* **2023**, *23*, 311. [CrossRef] [PubMed]
33. Demircan, N.; Cucun, G.; Uzilday, B. Mitochondrial Alternative Oxidase (AOX1a) Is Required for the Mitigation of Arsenic-Induced Oxidative Stress in *Arabidopsis thaliana*. *Plant Biotechnol. Rep.* **2020**, *14*, 235–245. [CrossRef]
34. Zeng, Y.; Tan, X.; Zhang, L.; Long, H.; Wang, B.; Li, Z.; Yuan, Z. A Fructose-1,6-Biphosphate Aldolase Gene from *Camellia oleifera*: Molecular Characterization and Impact on Salt Stress Tolerance. *Mol. Breed.* **2015**, *35*, 17. [CrossRef]
35. Lin, P.; Wang, K.; Wang, Y.; Hu, Z.; Yan, C.; Huang, H.; Ma, X.; Cao, Y.; Long, W.; Liu, W.; et al. The Genome of Oil-*Camellia* and Population Genomics Analysis Provide Insights into Seed Oil Domestication. *Genome Biol.* **2022**, *23*, 14. [CrossRef]
36. Hu, Z.; Zhang, M.; Wen, Q.; Wei, J.; Yi, H.; Deng, X.; Xu, X. Abnormal Microspore Development Leads to Pollen Abortion in a Seedless Mutant of 'Ougan' Mandarin (*Citrus suavissima* Hort. Ex Tanaka). *J. Am. Soc. Hortic. Sci.* **2007**, *132*, 777–782. [CrossRef]
37. Wang, R.; Fang, Y.-N.; Wu, X.-M.; Qing, M.; Li, C.-C.; Xie, K.-D.; Deng, X.-X.; Guo, W.-W. The miR399-*CsUBC24* Module Regulates Reproductive Development and Male Fertility in *Citrus*. *Plant Physiol.* **2020**, *183*, 1681–1695. [CrossRef]
38. Wei, C.; Zhang, R.; Yue, Z.; Yan, X.; Cheng, D.; Li, J.; Li, H.; Zhang, Y.; Ma, J.; Yang, J.; et al. The Impaired Biosynthetic Networks in Defective Tapetum Lead to Male Sterility in Watermelon. *J. Proteom.* **2021**, *243*, 104241. [CrossRef] [PubMed]
39. Luo, D.; Xu, H.; Liu, Z.; Guo, J.; Li, H.; Chen, L.; Fang, C.; Zhang, Q.; Bai, M.; Yao, N.; et al. A Detrimental Mitochondrial-Nuclear Interaction Causes Cytoplasmic Male Sterility in Rice. *Nat. Genet.* **2013**, *45*, 573–577. [CrossRef]
40. Falasca, G.; D'Angeli, S.; Biasi, R.; Fattorini, L.; Matteucci, M.; Canini, A.; Altamura, M.M. Tapetum and Middle Layer Control Male Fertility in *Actinidia deliciosa*. *Ann. Bot.* **2013**, *112*, 1045–1055. [CrossRef]
41. Papini, A.; Mosti, S.; Van Doorn, W.G. Classical Macroautophagy in Lobivia Rauschii (Cactaceae) and Possible Plastidial Autophagy in *Tillandsia albida* (Bromeliaceae) Tapetum Cells. *Protoplasma* **2013**, *251*, 719–725. [CrossRef]
42. Van Aken, O.; Van Breusegem, F. Licensed to Kill: Mitochondria, Chloroplasts, and Cell Death. *Trends Plant Sci.* **2015**, *20*, 754–766. [CrossRef] [PubMed]
43. Liu, Z.; Shi, X.; Li, S.; Hu, G.; Zhang, L.; Song, X. Tapetal-Delayed Programmed Cell Death (PCD) and Oxidative Stress-Induced Male Sterility of *Aegilops uniaristata* Cytoplasm in Wheat. *Int. J. Mol. Sci.* **2018**, *19*, 1708. [CrossRef] [PubMed]
44. Liu, Y.; Zhou, B.; Khan, A.; Zheng, J.; Dawar, F.U.; Akhtar, K.; Zhou, R. Reactive Oxygen Species Accumulation Strongly Allied with Genetic Male Sterility Convertible to Cytoplasmic Male Sterility in Kenaf. *Int. J. Mol. Sci.* **2021**, *22*, 1107. [CrossRef]
45. Deng, M.-H.; Wen, J.-F.; Huo, J.-L.; Zhu, H.-S.; Dai, X.-Z.; Zhang, Z.-Q.; Zhou, H.; Zou, X.-X. Relationship of Metabolism of Reactive Oxygen Species with Cytoplasmic Male Sterility in Pepper (*Capsicum annuum* L.). *Sci. Hortic.* **2012**, *134*, 232–236. [CrossRef]
46. Serrano, I.; Romero-Puertas, M.C.; Sandalio, L.M.; Olmedilla, A. The Role of Reactive Oxygen Species and Nitric Oxide in Programmed Cell Death Associated with Self-Incompatibility. *J. Exp. Bot.* **2015**, *66*, 2869–2876. [CrossRef] [PubMed]
47. Bai, Z.; Ding, X.; Zhang, R.; Yang, Y.; Wei, B.; Yang, S.; Gai, J. Transcriptome Analysis Reveals the Genes Related to Pollen Abortion in a Cytoplasmic Male-Sterile Soybean (*Glycine max* (L.) Merr.). *Int. J. Mol. Sci.* **2022**, *23*, 12227. [CrossRef]
48. Vermot, A.; Petit-Härtlein, I.; Smith, S.M.E.; Fieschi, F. NADPH Oxidases (NOX): An Overview from Discovery, Molecular Mechanisms to Physiology and Pathology. *Antioxidants* **2021**, *10*, 890. [CrossRef]
49. Chen, X. The Calcium Distribution in the Anther of Yunnan Purple Cytoplasmic Male Sterile Rice during anther Anther Development. Master's Thesis, Wuhan University, Wuhan, China, 2006.
50. Yang, S.J.; Liang, W.Y.; Shi, J.; Peng, L.; Zheng, R. Calcium Distribution during Anther Development in Impatiens *Balsamina*. *Biol. Plant.* **2020**, *64*, 178–184. [CrossRef]

Disclaimer/Publisher's Note: The statements, opinions and data contained in all publications are solely those of the individual author(s) and contributor(s) and not of MDPI and/or the editor(s). MDPI and/or the editor(s) disclaim responsibility for any injury to people or property resulting from any ideas, methods, instructions or products referred to in the content.